# Observation and Interpretation of Temperature-Dependent Valence Delocalization in the [2Fe−2S]$^{+}$ Cluster of a Ferredoxin from *Clostridium pasteurianum*

**Catalina Achim,[†] Emile L. Bominaar,*[,†] Jacques Meyer,[‡] Jim Peterson,[†] and Eckard Münck*[,†]**

*Contribution from the Department of Chemistry, Carnegie Mellon University, 4400 Fifth Avenue, Pittsburgh, Pennsylvania 15213, and Département de Biologie Moléculaire et Structurale, CEA−Grenoble, 38054 Grenoble, France*

*Received November 17, 1998*

**Abstract:** We present the results of Mössbauer and magnetization studies of [2Fe−2S]$^{+}$ clusters from the wild-type and the C56S variant 2Fe-ferredoxin from *Clostridium pasteurianum.* At pH = 11 in Tris/Caps buffer, samples of the C56S variant contain, at 4.2 K, a 1:1 mixture of [2Fe−2S]$^{+}$ clusters with valence-localized $S = {}^1/_2$ ($Fd_{1/2}$) and valence-delocalized $S = {}^9/_2$ ($Fd_{9/2}$) ground states. A spin Hamiltonian analysis of Mössbauer spectra recorded in applied fields up to 8.0 T provides the fine structure and hyperfine parameters for $Fd_{9/2}$: $D_{9/2} = -1.5$ cm$^{-1}$, $E/D = 0.11$, $\mathbf{A} = (-13, -13, -9.1)$ MHz, $\Delta E_Q = 1.83$ mm/s, $\eta = 0$, and $\delta = 0.50$ mm/s. A comparative analysis of the hyperfine tensor components for $Fd_{9/2}$ and $Fd_{1/2}$ shows that the intrinsic *A*-values cannot be directly transferred from localized to delocalized systems. This result indicates that valence delocalization is accompanied by additional modifications in the electronic structure. High-temperature Mössbauer studies show an increase in the fraction of valence-delocalized clusters, from ca. 50% at 4.2 K to ca. 94% at 200 K. Magnetic susceptibility studies rule out that the delocalized fraction generated at high temperature results from a spin conversion of $Fd_{1/2}$ to $Fd_{9/2}$. Rather, the change in the delocalized fraction is due to a rapid increase in the intramolecular electron-transfer rate between the two iron sites of $Fd_{1/2}$. Such a localization-to-delocalization transition has not been observed previously for any Fe−S cluster. The spectral features and the temperature range of the transition (≈100 K) suggest a distribution in the rate of electron transfer between the iron sites of $Fd_{1/2}$ and point toward a dispersion in the values for the electronic parameters arising from the interaction of the cluster with the protein in different conformations. The rate for electron transfer between the iron sites of $Fd_{1/2}$ was calculated using a quantum mechanical method which takes into account Heisenberg−Dirac−van Vleck exchange, spin-dependent resonance interaction, and vibronic trapping. By assuming a distribution in the parameters characterizing these interactions, we have been able to model the temperature dependence of the fraction of delocalized $Fd_{1/2}$ molecules. Our studies suggest that electron-transfer rates in Fe−S clusters from ferredoxins may probe the conformational substates of the protein moiety.

## Introduction

Fe−S clusters are common cofactors in electron-transfer (ET) proteins.[1] This function implies that Fe−S clusters support different oxidation states, including those of mixed-valence type. The latter states can be viewed as an ensemble of homovalent metal sites, accommodating a number of "extra" electrons. The smallest units which afford mixed-valence states are binuclear clusters. In these systems, the resonance interaction between the metal sites favors states in which the extra electron is delocalized over the metal sites. Vibronic interactions, however, can diminish the resonance interaction to a much weaker process, that is, of tunneling through a reorganizational potential barrier which separates valence-localized states.[2] Low electron-transfer rates on the time scale of a given spectroscopy give rise to spectra containing distinguishable contributions pertaining to the individual metal sites (i.e., "valence-localized" spectra).

In the presence of paramagnetic sites, the extra electron determines an intricate relationship between spin and intramolecular ET that is based on an approximate proportionality between resonance interaction and the total spin of the cluster.[3−5] This proportionality determines an increase in the ET rates for the individual spin levels of an exchange-coupled cluster as a function of the total spin.[2] Therefore, intracluster ET depends critically on the order of the spin levels. The level order is imposed by the relative magnitude of spin-dependent resonance interaction, antiferromagnetic Heisenberg−Dirac−van Vleck (HDvV) exchange, and vibronic coupling.[3] Thus, in class II dimers, both the increase in ET rate with the total spin and the ferromagnetic spin-coupling terms of double-exchange type are manifestations of resonance interaction, in the barrier range and at the potential minima, respectively. Biological ET involving clusters depends on the kinetic and thermodynamic effects

[†] Carnegie Mellon University.
[‡] CEA−Grenoble.

(1) Beinert, H.; Holm, R. H.; Münck, E. *Science* **1997**, *277*, 653−659.
(2) Bersuker, I. B.; Borshch, S. A. *Adv. Chem. Phys.* **1992**, *LXXXI*, 703−782.
(3) Borshch, S. A.; Bominaar, E. L.; Blondin, G.; Girerd, J.-J. *J. Am. Chem. Soc.* **1993**, *115*, 5155−5168.
(4) Anderson, P. W.; Hasegawa, H. *Phys. Rev.* **1955**, *100*, 675−681.
(5) Blondin, G.; Girerd, J.-J. *Chem. Rev.* **1990**, *90*, 1359−1376.

10.1021/ja983980k CCC: $18.00 
Published on Web 03/31/1999

associated with the most characteristic attributes of these systems, namely spin coupling and fractional metal valency.[6,7]

Studies of synthetic and protein-bound Fe−S clusters have indicated that the fine details of cluster structure and concomitant ground spin state are properties sensitive to the cluster environment.[8−11] Hendrickson et al. have argued that the environment of mixed-valence synthetic clusters in crystalline structure has an essential influence on their intramolecular ET rates.[12] Changes in the charge ordering with temperature have been proposed as the mechanism for the localization-to-delocalization transition observed for these mixed-valence solids. To the present, temperature-induced transition to delocalization has not been observed for any Fe−S cluster.

Mössbauer spectroscopic studies of mononuclear iron proteins have revealed the existence of appreciable heterogeneity at the cofactor binding sites.[13−15] One of the dynamic parameters obtained from these studies is the Lamb−Mössbauer factor, which depends on the mean-square displacement $\langle x^2\rangle_{Fe}$ of the $\gamma$-ray-absorbing $^{57}$Fe nuclei. The temperature dependence of $\langle x^2\rangle_{Fe}$ has been interpreted as arising from an energy distribution of protein substates. Studies of CO-rebinding rates[16] and "hole-burning" experiments,[17] as well as theoretical studies,[18] have provided additional evidence for the notion of an "energy landscape" in proteins consisting of a hierarchy of conformational substates organized in tiers.[19]

The electronic spins of the $Fe^{3+}$ and $Fe^{2+}$ sites of [2Fe−2S]$^{+}$ clusters in wild-type (WT) 2Fe-ferredoxin from *Clostridium pasteurianum* (2Fe*Cp*Fd) are antiferromagnetically coupled to yield a ground state with $S = {}^1/_2$.[1] This state is valence localized on the time scale of Mössbauer spectroscopy, indicating ET rates slower than the nuclear precession of $^{57}$Fe.

For a long time it has been widely accepted that there are sizable metal−metal interactions in [2Fe−2S]$^{+}$ clusters, despite the valence localization of these systems.[20] Recently, this notion has been corroborated by spectroscopic studies of [2Fe−2S]$^{+}$ clusters in C56S and C60S variants of 2Fe*Cp*Fd, in which one of the cysteinyl ligands is replaced by a serine.[21,22] According to MCD, EPR,[21a] and Mössbauer studies,[22] samples of these variants are physical mixtures of two species, one with a spin $S = {}^1/_2$ ($Fd_{1/2}$) and the other with a $S = {}^9/_2$ ($Fd_{9/2}$) ground state. Interestingly, the spin of the ground state correlates with the metal valencies: thus, $Fd_{1/2}$ is valence-localized ($Fe^{2+}-Fe^{3+}$), and $Fd_{9/2}$ is valence-delocalized ($Fe^{2.5+}-Fe^{2.5+}$).[22] This correlation demonstrates the double-exchange hypothesis, viz., that resonance delocalization leads to parallel spin ordering.[4] However, a precise knowledge of the nature of valence delocalization in $Fd_{9/2}$ is lacking. In particular, it is not yet clear whether $Fd_{9/2}$ is a class II compound[23] with fast electron transfer on the Mössbauer time scale or a class III compound. On the basis of an extrapolated value for the metal−metal resonance parameter in plant-type ferredoxins, Gamelin et al. have inferred that the $S = {}^9/_2$ excited state of these ferredoxins is fully delocalized (class III).[24] Since the ground state of $Fd_{9/2}$ must result from a rearrangement of the spin levels in the WT cluster, the $S = {}^9/_2$ ground state in the mutant cluster is probably class III as well.

In this study we investigate the temperature dependence of the Mössbauer spectra of the $Fd_{1/2}-Fd_{9/2}$ mixtures in samples of the C56S mutant. It is found that $Fd_{1/2}$ undergoes a gradual transition to a delocalized valence state by raising the temperature. This result constitutes the first observation of a localization-to-delocalization transition in a mixed-valence 2Fe-ferredoxin. The transition is not accompanied by any atypical changes in the $^{57}$Fe recoilless fraction or in the magnetic moment. However, the transition is not of the common merging type, but a clearly identifiable, though diminishing, valence-localized spectroscopic species is present throughout the transition range. To explain this remarkable observation, we explore a model based on the purported effect of a heterogeneous protein environment on the electronic structure of the cluster.

## Experimental Section

Tris/Caps samples were prepared from $^{57}$Fe-enriched protein solutions containing 200 mM NaCl in 20 mM Tris, pH = 8.0. The pH was adjusted to 10 < pH < 11 by adding 500 mM Caps buffer, pH = 11, to a final Caps concentration of 50 mM. The susceptibility samples were reduced using $Na_2S_2O_4$ in a 2:1 molar excess. Bicine/Pipes samples were prepared from $^{57}$Fe-enriched protein solutions containing 200 mM NaCl, 10 mM Pipes, 10 mM Bicine at pH = 7.5. To reach the indicated pH values, solutions of 50 mM Pipes, 50 mM Bicine of the following pH's were added to the protein solution: pH = 5.85 for a final pH of 6.7 (0.3:1 vol added buffer/vol protein solution), pH = 12.2 for a final pH of 8.7 (0.15:1 v/v), and pH = 12.2 for a final pH of 11.3 (0.5:1 v/v). Reduction of these samples was performed using dithionite solutions prepared in Bicine/Pipes buffers of the same pH as the samples. After Mössbauer analysis of the pH = 11.3 sample, a 500 mM Caps pH = 11 buffer was added to a final Caps concentration of 50 mM.

Lyophilization of dithionite-reduced samples of the C56S variant was performed in a Schlenck line. Samples were contained in Lucite Mössbauer cups, which allowed us to observe when the dehydration was complete. Freshly sublimed adamantane was added to the samples, which were then closed with a Lucite lid. Samples were sealed with silicone grease, frozen, and stored in liquid nitrogen.

**Magnetization Measurements.** Magnetization measurements were performed in a Quantum Design MPMS SQUID magnetometer, calibrated with an NBS Pd standard. Samples were contained in boron

(6) Achim, C.; Bominaar, E. L.; Münck, E. *J. Biol. Inorg. Chem.* **1997**, *3*, 126−134.
(7) Bominaar, E. L.; Achim, C.; Borshch, S. A.; Girerd, J.-J.; Münck, E. *Inorg. Chem.* **1997**, *36*, 3689−3701.
(8) Carney, M. J.; Papaefthymiou, G. C.; Spartalian, K.; Frankel, R. B.; Holm, R. H. *J. Am. Chem. Soc.* **1988**, *110*, 6084−6095.
(9) Lindahl, P. A.; Day, E. P.; Kent, T. A.; Orme-Johnson, W. H.; Münck, E. *J. Biol. Chem.* **1985**, *260*, 11160−11173.
(10) Meyer, J.; Moulis, J. M.; Gaillard, J.; Lutz, M. In *Advances in Inorganic Chemistry*; Cammack, R., Ed.; Academic Press: San Diego, CA, 1992; Vol. 38, pp 74−116.
(11) Hales, B. J.; Langosch, D. J.; Case, E. E. *J. Biol. Chem.* **1986**, *261*, 15301−15306.
(12) Hendrickson, D. N. *Mixed Valency Systems: Application in Chemistry, Physics, and Biology*; Kluwer Academic Publisher: Dordrecht, 1991; Vol. 343, pp 67−90.
(13) Parak, F.; Frolov, E. N.; Mössbauer, R. L.; Goldanskii, V. I. *J. Mol. Biol.* **1981**, *145*, 825−833.
(14) Parak, F.; Knapp, E. W.; Kucheida, D. *J. Mol. Biol.* **1982**, *161*, 177−194.
(15) Debrunner, P. G.; Frauenfelder, H. *Annu. Rev. Phys. Chem.* **1982**, *33*, 283−299.
(16) Austin, R. H.; Beeson, K. W.; Eisenstein, L.; Frauenfelder, H.; Gunsalus, I. C. *Biochemistry* **1975**, *14*, 5355−5373.
(17) Köhler, W.; Friedrich, J. *J. Chem. Phys.* **1989**, *90*, 1270−1273.
(18) Brooks, C. L., III, Karplus, M., Pettitt, B. M., Eds. *Proteins, A Theoretical Perspective of Dynamics, Structure, and Thermodynamics*; Wiley: New York, 1988.
(19) Onuchic, J. N.; Luthey-Schulten, Z.; Wolynes, P. G. *Annu. Rev. Phys. Chem.* **1997**, *48*, 545−600.
(20) Noodleman, L.; Baerends, E. J. *J. Am. Chem. Soc.* **1984**, *106*, 2316−2327.
(21) (a) Crouse, B. R.; Meyer, J.; Johnson, M. K. *J. Am. Chem. Soc.* **1995**, *117*, 9612−9613. (b) Golinelli, M.-P.; Chatelet, C.; Duin, E. C.; Johnson, M. K.; Meyer, J. *Biochemistry* **1998**, *37*, 10429−10437.
(22) Achim, C.; Golinelli, M.-P.; Bominaar, E. L.; Meyer, J.; Münck, E. *J. Am. Chem. Soc.* **1996**, *118*, 8168−8169.
(23) Robin, M. B.; Day, P. *Adv. Inorg. Chem. Radiochem.* **1967**, *10*, 247−422.
(24) Gamelin, D. R.; Bominaar, E. L.; Kirk, M. L.; Wieghardt, K.; Solomon, E. I. *J. Am. Chem. Soc.* **1996**, *118*, 8085−8097.

nitride cups, which allowed the collection of magnetization and Mössbauer data without protein transfer. Prior to filling, the cups were etched in 10% HF for 10 min to remove surface paramagnetic impurities. The samples were introduced quickly in the antechamber of the SQUID instrument, followed by purging of the sample space with He gas. To further reduce the risk of oxygen contamination, the sample space was flushed with He between succesive data points at temperatures above 150 K.

Magnetization studies of metalloproteins are potentially subject to serious errors pertaining to paramagnetic contributions from slowly relaxing, thermally nonequilibrated protons.[25] Fortunately, the susceptibility measurements on the C56S samples did not require deuteration of the samples because the proton contribution to the total magnetization was small compared to the electronic contribution. For example, the estimated proton susceptibility of a representative sample is $10^{-3}$ $\mu$J/T$^2$ at 20 K, which is negligible compared to the $Fd_{9/2}$ susceptibility, $\sim$0.9 $\mu$J/T$^2$. Indeed, thermal hysteresis was not observed in our measurements. For example, the magnetization data obtained at 4 T and 10 K from measurements that were interspersed by time intervals of a few hours coincided within 0.2%.

The high-temperature data ($T > 100$ K) were plotted as $\chi T$ vs $T$ curves that were fit using the Curie law, including a diamagnetic correction: $\chi T = C_{para} + \chi_{dia} T$, where $C_{para}$ is the Curie constant. At each value of the applied field, $H$, the paramagnetic magnetization was obtained by subtracting the fit value for $\chi_{dia} H$ from the raw magnetization data. The data were corrected for paramagnetic impurities in the cups and buffers.[25]

**Mössbauer Spectroscopy.** Mössbauer spectra were collected on constant-acceleration spectrometers. All isomer shifts are reported with respect to iron metal at room temperature. Data were analyzed using WMOSS software (WEB Research Co., Edina, MN).

The temperature dependence of the mean-square displacement $\langle x^2 \rangle_{Fe}$ was determined from the Lamb−Mössbauer factor $f = \exp(-4\pi^2 \langle x^2 \rangle_{Fe} / \lambda^2)$, a factor sensitive to dynamic processes that occur within $10^{-7}$ s, the characteristic time for resonance Mössbauer absorption. Here, $\lambda$ is the wavelength of the 14.4-keV nuclear transition of $^{57}$Fe ($\lambda = 0.86$ Å). The $f$-factor was evaluated at every temperature from the absorption area of the spectrum divided by the counting rate far off resonance. The absorption area is proportional to $f$, Area $= C_\gamma f$, where $C_\gamma$ is a constant which depends on the amount of $^{57}$Fe in the sample. The temperature dependence of $\langle x^2 \rangle_{Fe}$ is linear between 50 and 150 K, indicating classical behavior. This implies that extrapolation of the temperature dependencies of $\langle x^2 \rangle_{Fe}$ and ln(Area) to $T = 0$ yields the limiting values $\langle x^2 \rangle_{Fe} = 0$ and ln(Area) $=$ ln($C_\gamma$). Thus, by subtracting ln($C_\gamma$) from ln(Area), we obtain the temperature-dependent part of $\langle x^2 \rangle_{Fe}$. The extrapolation procedure yielded the value $\langle x^2 \rangle_{Fe} = 0.00253$ Å$^2$ at 4.2 K, which is comparable with the values 0.00418 and 0.00124 Å$^2$ reported by Parak et al. for deoxymyoglobin and metmyoglobin, respectively.[13,14] A background correction for non-14.4-keV radiation was not required; this correction affects the value of $C_\gamma$ but does not influence the results for the temperature-dependent part of $\langle x^2 \rangle_{Fe}$.

## Results and Analysis

**Solvent Effects.** Because our samples contain a mixture of $Fd_{9/2}$ and $Fd_{1/2}$, the analysis of the magnetization and Mössbauer data requires the deconvolution of the contributions for these species. In an effort to obtain samples containing pure $Fd_{9/2}$ species, we have investigated physical and chemical factors likely to influence the $Fd_{9/2}$:$Fd_{1/2}$ ratio. We did not find any effect of factors such as incubation time after glycerol addition, freezing time, order of glycerol addition and reduction, and protein concentration. A summary of the $Fd_{9/2}$:$Fd_{1/2}$ ratios depending on pH, buffer, or glycerol concentration is given in Table 1.

Examination of the data in Table 1 reveals a complex influence of these factors on the $Fd_{9/2}$:$Fd_{1/2}$ ratio. $Fd_{9/2}$ is not formed in Bicine/Pipes buffers, in the pH range between 6.7 and 11.3. However, addition of Caps to solutions prepared in Bicine/Pipes led to formation of $Fd_{9/2}$ (entry 4 of Table 1). Protein solutions prepared at pH = 8.0 in Tris/HCl buffer contained small amounts of $Fd_{9/2}$ (less than 10%). Increasing the pH from 8 to $\sim$11, by addition of Caps buffer, led to an increase in the amount of $Fd_{9/2}$ (see Table 1). Addition of glycerol to the samples had a pH-dependent effect on the $Fd_{9/2}$:$Fd_{1/2}$ ratio. At pH = 11, the $Fd_{9/2}$:$Fd_{1/2}$ ratio decreased upon glycerol addition. In contrast, at pH = 8, the $Fd_{9/2}$:$Fd_{1/2}$ ratio increased with the glycerol content of the samples up to 30% (v/v) and then decreased upon further addition of glycerol.

**Table 1.** Composition of Reduced C56S Samples

| pH | buffer | glycerol (%) | $Fd_{9/2}$:$Fd_{1/2}$[a] |
|---|---|---|---|
| 6.7 | Bicine/Pipes | 0 | 0 |
| 8.7 | Bicine/Pipes | 0 | 0 |
| 11.3 | Bicine/Pipes | 0 | 0 |
| 11 | Bicine/Pipes/Caps | 0 | 1.0(1) |
| 8 | Tris | 0 | 0.05(5) |
| 8 | Tris | 30 | 0.30(5) |
| 8 | Tris | 50 | 0.10(5) |
| 10 | Tris/Caps | 0 | 0.40(5) |
| 11 | Tris/Caps | 0 | 1.0(1)[b] |
| 11 | Tris/Caps | 30 | 0.60(8) |
| 11 | Tris/Caps | 50 | 0.42(5) |

[a] The $Fd_{9/2}$:$Fd_{1/2}$ ratios represent averages of samples prepared under the conditions indicated. Numbers in parentheses indicate the spread in the $Fd_{9/2}$:$Fd_{1/2}$ ratios for different samples. [b] Sample used for the magnetization and Mössbauer studies.

It is apparent that the pH influences the formation of $Fd_{9/2}$ in the presence of Tris or Caps. We note that Tris and Caps, in the presence of which $Fd_{9/2}$ is generated, contain a primary amine, while Bicine and Pipes contain a tertiary, sterically hindered amine. Thus, Tris and Caps could possibly coordinate to the iron sites of the [2Fe−2S] cluster (which is located relatively close to the protein surface[21b]). Coordination of buffer molecules to metal sites in proteins would not be an unprecedented finding.[26] Interaction of buffer molecules with groups at the protein surface and, possibly, subsequent changes in the protein conformation could be an alternative explanation for the formation of clusters of the $Fd_{9/2}$ type. This explanation, which relies on the interaction between buffer molecules and the protein surface, would be supported by the observation of the glycerol effect on the $Fd_{9/2}$:$Fd_{1/2}$ ratio. Further investigations of the factors controlling the $Fd_{9/2}$:$Fd_{1/2}$ ratio are in progress.

**Mössbauer Spectroscopy.** In a Communication in this journal,[22] we reported the results of a low-field, low-temperature Mössbauer study of the C56S variant of 2Fe*Cp*Fd. This study confirmed that reduced samples contain a mixture of $Fd_{9/2}$ and $Fd_{1/2}$ species, and it unambiguously established that the extra electron is delocalized in $Fd_{9/2}$ (down to 1.5 K) and localized in $Fd_{1/2}$. In the following, we present the results of variable-field, variable-temperature Mössbauer measurements.

Figure 1C−E shows 4.2 K Mössbauer spectra of the dithionite-reduced C56S variant recorded in applied magnetic fields of 0.05, 5.0, and 8.0 T. The solid lines through the experimental data are the sum of spectral simulations for $Fd_{9/2}$ and $Fd_{1/2}$ which are based on the spin Hamiltonian in eq 1 using the hyperfine parameters listed in Table 2. The table gives also the spin

(25) Day, E. P. *Methods Enzymol.* **1993**, *227*, 437−463.

(26) Rosenzweig, A. C.; Lippard, S. J. *Acc. Chem. Res.* **1994**, *27*, 229−236.

**Table 2.** Hyperfine Parameters at 4.2 K for WT and C56S [2Fe−2S]$^{+}$ Clusters

| cluster | | $\Delta E_Q$ (mm/s) | $\eta^a$ | $\delta$ (mm/s) | $A_x$ (MHz) | $A_y$ (MHz) | $A_z$ (MHz) |
|---|---|---|---|---|---|---|---|
| WT | $Fe^{3+}$ | −1.0(1) | −2.0(3) | 0.34(2) | −57(2) | −41(2) | −49(2) |
| | $Fe^{2+}$ | +3.2(1) | 0.2(2) | 0.65(3) | 28(3) | 32(3) | 9.7(2) |
| $Fd_{1/2}$ | $Fe^{3+}$ | −1.0(1) | −1.5(3) | 0.32(2) | −51(2) | −44(2) | −50(2) |
| | $Fe^{2+}$ | +3.1(1) | 0.3(2) | 0.73(4) | 25(3) | 30(3) | 5.6(2) |
| $Fd_{9/2}$ | $Fe^{2.5+}$ | +1.84(5) | 0 | 0.53(3) | −12.7(3) | −12.7(3) | −8.9(2) |
| | $Fe^{2.5+}$ | +1.81(4) | 0[b] | 0.47(3) | −13.3(3) | −13.3(3) | −9.3(1) |

[a] The *x*, *y*, and *z* axes of **V**- and **A**-tensors coincide. For the $Fe^{2+}$ and $Fe^{2.5+}$ sites, the convention was adopted that $|V_{zz}| \geq |V_{yy}| \geq |V_{xx}|$. [b] Best fits of the spectra were obtained when the *z*-axis of the EFG-tensor is rotated 10(1)° with respect to the *z*-axis of the **A**-tensor.

Hamiltonian parameters obtained for the mixed-valence [2Fe−2S]$^{+}$ cluster in the WT protein.

$$H = D\{\mathbf{S}_z^2 - S(S+1)/3 + (E/D)(\mathbf{S}_x^2 - \mathbf{S}_y^2)\} + \mu_B \mathbf{H}\cdot\mathbf{g}\cdot\mathbf{S} + \sum_{i=1,2}\{\mathbf{S}\cdot\mathbf{A}(i)\cdot\mathbf{I}_i - g_N\mu_N\mathbf{H}\cdot\mathbf{I}_i + eQ\mathbf{I}_i\cdot\mathbf{V}_i\cdot\mathbf{I}_i\} \quad (1)$$

In eq 1, $S$ is the cluster spin, $D$ is the zero-field splitting parameter, $E$ is the rhombicity parameter, $\mu_B$ and $\mu_N$ are the Bohr and nuclear magnetons, **A** is the magnetic hyperfine tensor, and **V** is the electric field gradient (EFG) tensor. The summation is over the two metal sites of the cluster.

We studied a variety of Fd samples with EPR and identified the spectra of $Fd_{9/2}$ and $Fd_{1/2}$. Simulations of the $Fd_{9/2}$ spectrum showed $D_{9/2} < 0$ and $E/D = 0.11(1)$, in good agreement with previous reports.[21a,27] Moreover, the simulations showed $g_x = 2.03$, $g_y = 2.03$, and $g_z = 2.03$. Mössbauer and magnetization studies provided the value for $D_{9/2} = -1.5$ cm$^{-1}$ (see below). For this value, the first excited Kramers doublet of the $S = {}^9/_2$ multiplet is 12.0 cm$^{-1}$ above the ground state, and, therefore, only the ground doublet of the $S = {}^9/_2$ system is appreciably populated at 4.2 K. In applied fields of moderate strength, the ground doublet exhibits uniaxial magnetization behavior ($\langle S_x\rangle = -0.02$, $\langle S_y\rangle = -0.01$, $\langle S_z\rangle = -4.49$). Under these conditions, only the components of the **A**-tensors along the electronic *z*-axis can be determined. The spectrum of each iron site of such an uniaxial system consists of six absorption lines with relative intensities 3:2:1:1:2:3. The outermost lines are the most easily identifiable ones when $Fd_{9/2}$ occurs in mixtures with $Fd_{1/2}$. As can be seen in Figure 1A−C, the rightmost line of $Fd_{9/2}$ lies outside the $Fd_{1/2}$ spectrum and can be used for quantitating the $Fd_{9/2}$ species with high precision. Detailed analysis of the leftmost feature of the $Fd_{9/2}$ spectrum revealed two slightly inequivalent iron sites. As indicated in Figure 1B, these sites contribute to the leftmost feature two coinciding lines (a in Figure 1B) and a pair of two closely spaced lines (b in Figure 1B).

In strong applied fields, the spin expectation values along the *x* and *y* directions are larger due to interdoublet Zeeman mixing; e.g., at 8 T and for $E/D = 0.115$ and $D_{9/2} = -1.5$ cm$^{-1}$, the spin expectation values are $\langle S_x\rangle = -3.7$, $\langle S_y\rangle = -2.6$, and $\langle S_z\rangle = -4.5$. $\langle S_x\rangle$ and $\langle S_y\rangle$ depend quite sensitively on the magnitude of $D_{9/2}$. Hence, high-field Mössbauer spectroscopy in conjunction with spectral simulations provides a means for determining $D_{9/2}$, $A_x$, and $A_y$. The results of our analysis are summarized in Table 2. The value obtained for $D_{9/2}$ is −1.5(1) cm$^{-1}$. In a strongly coupled spin system, the zero-field splitting tensor $\mathbf{D}_{9/2}$ of the $S = {}^9/_2$ state can be expressed in terms of the tensors for the individual sites as $\mathbf{D}_{9/2} = ({}^5/_{18})\mathbf{D}(Fe^{3+}) + ({}^1/_6)\mathbf{D}(Fe^{2+})$. Typically, the values for $|D|$ in rubredoxins and $FeS_4$ model complexes range between 6 and 10 cm$^{-1}$ for $Fe^{2+}$ and between 1 and 2 cm$^{-1}$ for $Fe^{3+}$.[28] This yields for $|D_{9/2}|$ the range 0.5−2.2 cm$^{-1}$, which includes the experimental value.

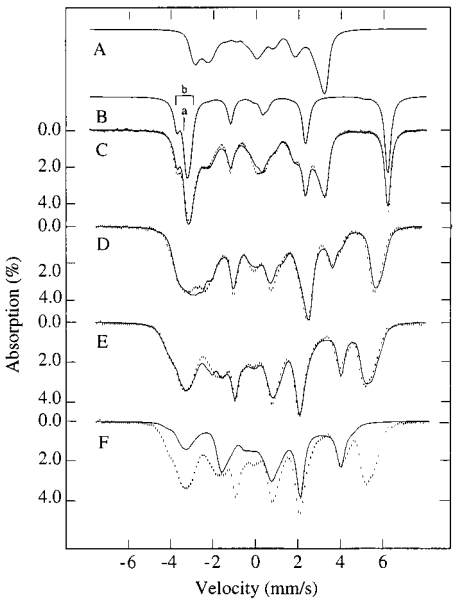


**Figure 1.** 4.2 K Mössbauer spectra recorded in applied magnetic fields of 0.05 (C), 5.0 (D), and 8.0 T (E,F). The fields were applied parallel to the $\gamma$-ray propagation. The solid lines drawn through the experimental data (C−E) represent the sum of calculated spectra for $Fd_{1/2}$ and $Fd_{9/2}$ using the spin Hamiltonian of eq 1 and the hyperfine parameters given in Table 2. The solid line drawn in F represents the $Fd_{1/2}$ contribution to the 8.0-T spectrum. Curves A and B represent the contributions of $Fd_{1/2}$ and $Fd_{9/2}$, respectively, to the spectrum of C. Lines marked a and b in spectrum B indicate the position of the leftmost lines for the two sites of the $Fd_{9/2}$ cluster.

The analysis of the $Fd_{1/2}$ spectra is based on eq 1, taking $D = E = 0$ and the values $g_1 = 1.88$, $g_2 = 1.92$, $g_3 = 2.01$ obtained from EPR. The strategy for analyzing spectra of mixed-valence [2Fe−2S]$^{+}$ clusters with a valence-localized $S = {}^1/_2$ ground state has been described in detail in a previous paper.[29] The antiferromagnetic coupling of $S = 2$ ($Fe^{2+}$) and $S = {}^5/_2$ ($Fe^{3+}$) to a resultant spin $S = {}^1/_2$ gives rise to magnetic hyperfine parameters with opposite signs for the two metal sites. As a consequence, the magnetic splitting of the $Fe^{2+}$ site increases with the applied magnetic field while the splitting of the $Fe^{3+}$ site decreases. These features allowed us to identify the rightmost line of the $Fe^{2+}$ site in the 8-T spectrum (Figure 1F). Detailed analysis shows that the asymmetry parameter $\eta$ and the **A**-tensor for the $Fe^{2+}$ site cannot be inferred from low-temperature Mössbauer studies alone (see ref 30). Under favorable conditions, the asymmetry parameter can be obtained from high-temperature, high-field spectra. However, the high-temperature properties of $Fd_{1/2}$ precluded this analysis, and only a family of ($\mathbf{A}$,$\eta$) solutions was obtained; the relatively large uncertainties quoted for $A_x$ and $A_y$ in Table 2 reflect the range of values determined for this family.

(27) Johnson, M. K.; Duin, E. C.; Crouse, B. R.; Golinelli, M.-P.; Meyer, J. In *Spectroscopic methods in bioinorganic chemistry*; Solomon, E. I., Hodgson, K. O., Eds.; ACS Symposium Series 692; American Chemical Society: Washington, DC, 1998; pp 286−301.

(28) Debrunner, P. G.; Münck, E.; Que, L.; Schulz, C. E. In *Iron−Sulfur Proteins*; Lovenberg, W., Ed.; Academic Press: New York, 1977; Vol. III, pp 381−418.

(29) Pikus, J. D.; Studts, J. M.; Achim, C.; Kauffmann, K. E.; Münck, E.; Steffan, R.; McClay, K.; Fox, B. G. *Biochemistry* **1996**, *35*, 9106−9119.

(30) Fox, B. G.; Hendrich, M. P.; Surerus, K. K.; Andersson, K. K.; Froland, W. A.; Lipscomb, J. D.; Münck, E. *J. Am. Chem. Soc.* **1993**, *115*, 3688−3701.

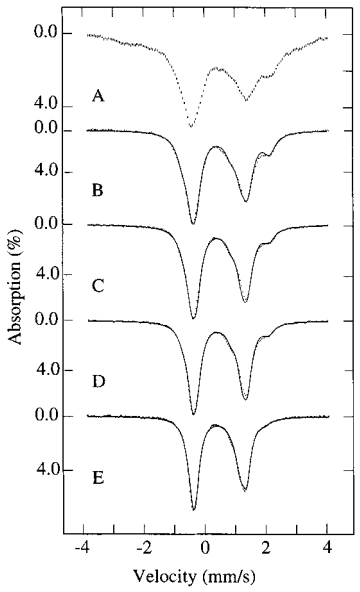


**Figure 2.** Zero-field Mössbauer spectra of $^{57}$Fe-reduced C56S 2Fe-ferredoxin (sample of Figure 1) collected at 75 (A), 106 (B), 133 (C), 150 (D), and 200 K (E). The solid lines drawn through the experimental data (B−E) represent the sum of quadrupole doublets with parameters given in Table 3.

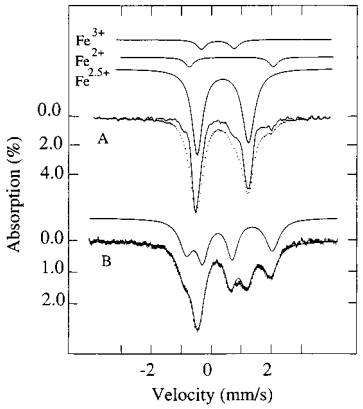


**Figure 3.** Zero-field Mössbauer spectra of reduced 2Fe-ferredoxin from the C56S variant collected at 150 K (A) and from the C60S variant collected at 200 K (B). The solid line in A represents the spectrum after removing the line width contribution of the $^{57}$Co source. Above spectrum A, the contributions for $Fe^{2+}$, $Fe^{3+}$, and $Fe^{2.5+}$ sites are shown. Above spectrum B, the sum of the contributions for the $Fe^{2+}$ and $Fe^{3+}$ sites of the valence-localized species is indicated.

Figure 2 shows Mössbauer spectra collected in zero field at temperatures between 75 and 200 K. Due to intermediate spin relaxation rates between 30 and 90 K, both $Fd_{1/2}$ and $Fd_{9/2}$ yield broad spectra (e.g., Figure 2A) which are difficult to analyze. However, above 90 K, the relaxation rates approach the fast fluctuation limit, whereupon the thermal spin expectation values approach zero according to Curie law. Under these conditions, the magnetic hyperfine interactions are averaged out, and the high-temperature Mössbauer spectra consist of doublets with isomer shifts and quadrupole splittings that reflect the oxidation states of the iron sites. Figure 3A shows the 150 K Mössbauer spectrum of the C56S variant. The traces drawn above the spectrum are the component spectra for the individual iron sites, obtained by deconvolution of the spectrum. $Fd_{1/2}$ appears as a 1:1 superposition of two distinct doublets (upper two traces), characteristic of the $Fe^{3+}$ and $Fe^{2+}$ sites of a valence-*localized* $[Fe_2S_2]^+$ cluster.[31] $Fd_{9/2}$ appears as one doublet (third trace), that is, as two coinciding doublets for the two equivalent $Fe^{2.5+}$ sites of the valence-*delocalized* $[Fe_2S_2]^+$ cluster. The quadrupole splitting and isomer shift of the $Fe^{2.5+}$ sites in $Fd_{9/2}$ are close to the arithmetic averages of the values for the $Fe^{2+}$ and $Fe^{3+}$ sites in $Fd_{1/2}$ (see Figure 2 and Table 3). Frequently, the spectral resolution can be improved by removing the line width contribution of the $^{57}$Co source by means of a Fourier transform technique.[33] The solid line drawn through the spectrum in Figure 3A was obtained by such a procedure. The ensuing sharpening of the spectral bands facilitates the determination of the quadrupole splittings and isomer shifts for the $Fe^{2.5+}$, $Fe^{2+}$, and $Fe^{3+}$ doublets. A three-doublet pattern similar to that observed for C56S can also be clearly discerned in the 200 K spectrum of the C60S variant species.

The sample of Figure 1, which contained a ca. 1:1 mixture of $Fd_{9/2}$ and $Fd_{1/2}$ at 4.2 K, was used for collecting the high-

**Table 3.** Temperature Dependence of Sample[a] Composition

| $T$ (K) | | $\delta^b$ (mm/s) | $\Delta E_Q{}^b$ (mm/s) | $\Gamma^b$ (mm/s) left | $\Gamma^b$ (mm/s) right | area (%) |
|---|---|---|---|---|---|---|
| 90 | $Fe^{2+}$ | 0.73 | 2.88 | 0.55 | 0.55 | 20(5) |
| | $Fe^{3+}$ | 0.34 | 1.14 | 0.55 | 0.55 | 18(5) |
| | $Fe^{2.5+}$ | 0.47 | 1.46 | 0.47 | 0.47 | 10(4) |
| | $Fe^{2.5+}$ | 0.51 | 1.82 | 0.53 | 0.53 | 50(3) |
| 106 | $Fe^{2+}$ | 0.72 | 2.86 | 0.46 | 0.46 | 16(4) |
| | $Fe^{3+}$ | 0.33 | 1.13 | 0.47 | 0.52 | 16(4) |
| | $Fe^{2.5+}$ | 0.48 | 1.45 | 0.39 | 0.39 | 16(4) |
| | $Fe^{2.5+}$ | 0.51 | 1.82 | 0.43 | 0.47 | 50(4) |
| 133 | | 0.72 | 2.80 | 0.45 | 0.45 | 11(3) |
| | | 0.33 | 1.11 | 0.43 | 0.43 | 11(3) |
| | | 0.48 | 1.50 | 0.37 | 0.40 | 28(3) |
| | | 0.49 | 1.83 | 0.41 | 0.45 | 50(3) |
| 150 | | 0.70 | 2.79 | 0.42 | 0.45 | 9.5(3) |
| | | 0.33 | 1.08 | 0.38 | 0.38 | 9.5(3) |
| | | 0.47 | 1.50 | 0.36 | 0.36 | 30(3) |
| | | 0.49 | 1.81 | 0.37 | 0.39 | 50(3) |
| 185 | | 0.69 | 2.58 | 0.39 | 0.39 | 6(2) |
| | | 0.32 | 1.10 | 0.38 | 0.38 | 6(2) |
| | | 0.44 | 1.49 | 0.35 | 0.35 | 38(3) |
| | | 0.48 | 1.78 | 0.36 | 0.36 | 50(3) |
| 200 | | 0.69 | 2.55 | 0.37 | 0.37 | 4(2) |
| | | 0.31 | 1.11 | 0.33 | 0.33 | 4(2) |
| | | 0.42 | 1.47 | 0.34 | 0.38 | 42(3) |
| | | 0.47 | 1.77 | 0.38 | 0.38 | 50(3) |

[a] The dithionite-reduced sample contained, at 4.2 K, a mixture of $Fd_{1/2}$ and $Fd_{9/2}$ in 1:1 molar ratio (pH ≈ 11, 16 mM Tris, 52 mM Caps, 6 mM $Na_2S_2O_4$, 155 mM NaCl). The second-order Doppler shift observed for the sum of all component spectra was −0.06 mm/s between 90 and 200 K. This temperature-induced change is typical for Fe-containing proteins. Due to the presence of multiple species, an accurate determination of the individual species $\delta$-values is difficult. In our simulations, we were guided by the requirement that the $\delta$-values of all components exhibit the expected second-order Doppler shift. [b] Typical precision for reported isomer shifts is ±0.04 mm/s and for quadrupole splittings is ±0.08 mm/s. $\Gamma$ is the full width at half-maximum.

(31) On the basis of MCD studies, Johnson and co-workers have suggested that the serine is coordinated at the reducible site of $Fd_{1/2}$.[27] We offer the following comments based on the present Mössbauer results. The $[2Fe-2S]^{2+}$ clusters in WT ferredoxin ($Cys_4$ coordination) and the C56S variant each exhibit *one* quadrupole doublet, with $\Delta E_Q = 0.67$ mm/s and $\delta = 0.28$ mm/s, and $\Delta E_Q = 0.53$ mm/s and $\delta = 0.28$ mm/s, respectively. Thus, the isomer shift, which is generally quite sensitive to oxidation state and coordination, does not indicate the presence of a special site. Interestingly, a C42S variant of *Cp* rubredoxin (Rd) exhibits $\delta = 0.27$ mm/s, while the WT Rd has $\delta = 0.24$ mm/s.[32] For the reduced C42S Rd, we observed $\delta = 0.78$ mm/s, which should be compared with $\delta = 0.70$ mm/s of the $Cys_4$-coordinated iron site of WT Rd. Thus, if one of the iron sites of $Fd_{1/2}$ has a noncysteine ligand, comparison of the isomer shifts listed in Table 2 would indicate that this ligand is coordinated at the reducible site.

(32) Yoo, S. J.; Achim, C.; Meyer, J.; Münck, E., unpublished results.

(33) Zimmermann, R.; Münck, E.; Brill, W. J.; Shah, V. K.; Henzl, M. T.; Rawlings, J.; Orme-Johnson, W. H. *Biochim. Biophys. Acta* **1978**, *537*, 185−207.

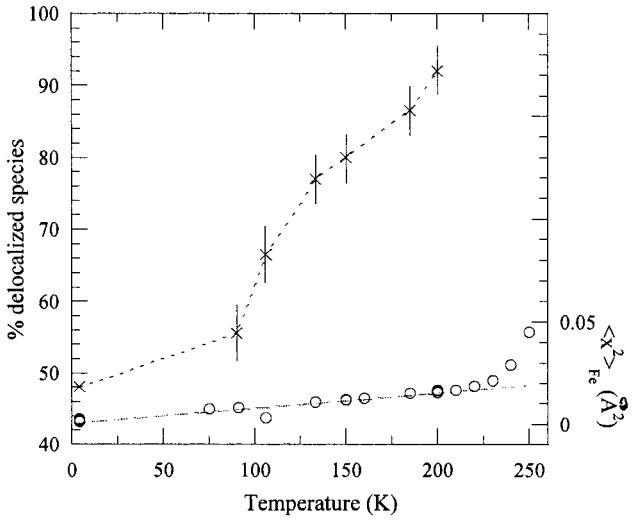


**Figure 4.** (Top) Temperature dependence of the fraction of delocalized species for the sample of Figures 1 and 2 (×). The curve is drawn only to guide the eye. The delocalized population at 4.2 K corresponds to $Fd_{9/2}$. (Bottom) Temperature dependence of the mean-square displacements $\langle x^2 \rangle_{Fe}$ of $^{57}$Fe nuclei for sample of Figure 1 (○). At temperatures above 250 K, the Lamb−Mössbauer factor was so low that measurements were precluded.

temperature spectra of Figure 2. On the basis of the low-temperature composition, one would expect the high-temperature spectra to be a superposition of three doublets corresponding to $Fe^{3+}$ (25%) and $Fe^{2+}$ (25%) in $Fd_{1/2}$, and $Fe^{2.5+}$ (50%) in $Fd_{9/2}$. Surprisingly, however, the delocalized fraction increases with temperature at the expense of the localized fraction. Eventually, nearly all iron in the sample (i.e., 92−96% at 200 K) can be represented by a quadrupole doublet with parameters characteristic for $Fe^{2.5+}$ ($\delta \approx 0.45$ mm/s and $\Delta E_Q \approx 1.7$ mm/s). Just as the simulations shown in Figure 3, those in Figure 2B−E are based on a weighted superposition of quadrupole doublets for the $Fe^{2+}$, $Fe^{3+}$, and $Fe^{2.5+}$ sites. Detailed analysis of the high-temperature data indicates that the contribution corresponding to $Fe^{2.5+}$ sites is best described by two doublets, namely one doublet with $\Delta E_Q = 1.8$ mm/s and temperature-independent intensity (50%) and one doublet with $\Delta E_Q = 1.5$ mm/s for which the intensity increases with the temperature. The optimized values for relative areas, line width, and hyperfine parameters used for the simulations of Figure 2 are listed in Table 3. The quadrupole splittings are virtually independent of temperature between 90 and 150 K. The widths of the absorption lines decrease in the same temperature interval as a result of increased spin relaxation rates. In Figure 4 we have plotted the delocalized fraction of the sample of Figures 1 and 2 as a function of the temperature. The plot reveals that the conversion to delocalization proceeds gradually. This behavior was not specific for this particular sample but was found to be a common property of all samples having sizable $Fd_{9/2}$ fractions at 4.2 K. Similar observations were made for the [2Fe−2S]$^{+}$ cluster of the C60S variant. The C60S sample for which the spectrum is shown in Figure 3B had an $Fd_{9/2}$:$Fd_{1/2}$ ratio of 0.15:0.85 at 4.2 K; at 200 K, 35% of the iron in the sample is contained in valence-delocalized clusters represented by the doublet with parameters characteristic of $Fe^{2.5+}$.

Analyses of samples prepared under different combinations of pH, buffer, and solvent composition revealed that the fraction of $Fd_{1/2}$ that converts into a delocalized form at high temperature is approximately proportional to the $Fd_{9/2}$:$Fd_{1/2}$ ratio at 4.2 K.[34]

(34) Achim, C.; Münck, E., unpublished results.

Thus, it appears that conditions which favor $Fd_{9/2}$ enhance the propensity of $Fd_{1/2}$ toward temperature-induced delocalization. 2Fe*Cp*Fd is a homodimer containing one cluster per subunit. It is possible that samples with less than 50% $Fd_{9/2}$ contain two slightly different $Fd_{1/2}$-type clusters. We speculate that only those $Fd_{1/2}$ clusters which reside in the same protein dimer with an $Fd_{9/2}$ cluster may undergo the localization-to-delocalization transition.

To assess the influence of solution conformations on the localization-to-delocalization transition of the $Fd_{1/2}$ form, we have conducted Mössbauer experiments on a lyophilized sample. For this purpose, we have chosen a glycerol-free sample containing a ca. 1:1 mixture of $Fd_{9/2}$ and $Fd_{1/2}$ and found that, after lyophilization, the ratio $Fd_{9/2}$:$Fd_{1/2}$ had changed to 1:2. The change shows once more that the electronic structure of clusters is affected by the protein. The high-temperature delocalized fraction of the lyophilized sample coincides with the low-temperature fraction up to 240 K. This is in contrast to the behavior in frozen protein solutions, where we observed an increase in the delocalized fraction with the temperature.

Figure 4 (lower panel) shows the mean-square displacement, $\langle x^2 \rangle_{Fe}$, obtained for a frozen protein solution of the C56S variant as a function of temperature (sample of Figures 1 and 2; see Experimental Section). The uncertainties were estimated from multiple measurements performed on different samples. The slope of $\langle x^2 \rangle_{Fe}$ vs $T$ changes abruptly around 220 K (see Figure 4), indicating thawing of frozen degrees of freedom. Similar behavior has been observed in Mössbauer studies of myoglobin, where it was attributed to activation of protein segmental motion.[13,15]

**Magnetic Susceptibility.** Figure 5 shows the results of magnetic susceptibility measurements performed on a sample containing, at 4.2 K, a ca. 1:1 mixture of $Fd_{9/2}$ and $Fd_{1/2}$. The measured quantity is the magnetization $M$, which at high temperature (i.e., for $kT \gg D$, $\mu_B H$) is a linear function of the field, $M = \chi H$. The magnetizations, $M_i$, of the various species in the sample are additive quantities, i.e., $M = \sum_i n_i M_i$, where $n_i$ is the molar amount of species $i$, and $\chi T = \sum_i n_i (\chi_i T)$. The relative contributions of $Fd_{1/2}$ and $Fd_{9/2}$ cannot be easily elicited from the magnetization data. Therefore, the molar fractions of the species at 4.2 K were determined by Mössbauer analysis of the susceptibility samples contained in boron nitride cups. This quantitation gave $n_{1/2}/n_{9/2} \approx 1$ for the sample of Figure 5. Mössbauer spectra also established that the sample was fully reduced and did not contain adventitiously bound $Fe^{2+}$ or $Fe^{3+}$.

Below 80 K, plots of the isofield data vs $\mu_B H/kT$ yielded a nested set of magnetization curves with various degrees of saturation (Figure 5B). Nesting and saturation are characteristic for species with $S > {}^1/_2$, i.e., $Fd_{9/2}$. These properties depend critically on the relative magnitudes of Zeeman splitting ($\sim \mu_B H$), thermal activation energy ($\sim kT$), and zero-field splitting ($\sim D_{9/2}$). For temperatures at which only the $S = {}^9/_2$ multiplet is significantly populated, the magnetization of $Fd_{9/2}$ is given by $M = -N\sum_{m=1}^{10}(\partial \epsilon_m/\partial H) \exp(-\epsilon_m/kT)/\sum_{m=1}^{10} \exp(-\epsilon_m/kT)$, where $\epsilon_m$ is the energy of the magnetic sublevel $m$ obtained by diagonalization of the spin Hamiltonian eq 1 in the $S = {}^9/_2$ manifold. The values for $E/D$ and **g** used in the simulation were determined by EPR: $E/D = 0.115$, **g** = (2.03, 2.03, 2.03). Magnetization curves for $Fd_{1/2}$ were calculated using the $g$-values determined from EPR: $g_1 = 1.88$, $g_2 = 1.92$, $g_3 = 2.01$. With the constraint on $n_{1/2}$:$n_{9/2}$ derived from Mössbauer analysis, there are only two free fit parameters, namely, $D_{9/2}$ and the amount of ferredoxin in the sample $n_{tot} = n_{1/2} + n_{9/2}$. The best fits were obtained for $D_{9/2} = -1.6(2)$ cm$^{-1}$, which is

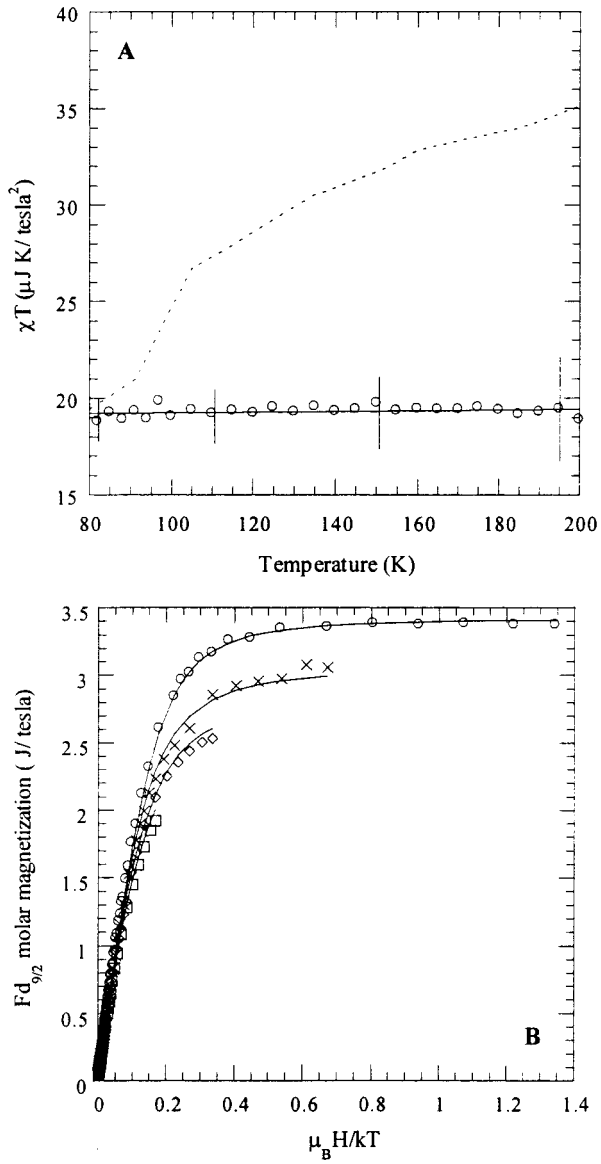


**Figure 5.** (A) High-temperature magnetic susceptibility data $\chi T$ vs $T$ plot for a 170-$\mu$L sample containing ca. 1:1 $Fd_{9/2}$:$Fd_{1/2}$ mixture. The uncertainties, indicated for a few data points, were estimated from four data sets measured at fields of 0.5, 1.0, 2.0, and 4.0 T. The solid line drawn through the data represents a fit of the experimental data to the curve $\chi T = 19.1(\mu J\ K\ T^{-2}) + 1.7\ 10^{-3}(\mu J\ T^{-2})T(K)$. The upper curve gives the calculated $\chi T$ values assuming a spin conversion of $Fd_{1/2}$ to $Fd_{9/2}$. (B) Magnetization curves for $Fd_{9/2}$. Data were collected at 4.0 (○), 2.0 (×), 1.0 (◇), and 0.5 T (□). The theoretical curves drawn through the data were calculated using the spin Hamiltonian of eq 1 with $D_{9/2} = -1.6\ cm^{-1}$, $E/D = 0.115$, and $\mathbf{g} = (2.03, 2.03, 2.03)$.

in very good agreement with the value obtained from the Mössbauer analysis.

We showed in the preceding section that the high-temperature Mössbauer spectra for $Fd_{1/2}$ (Figure 2) are nearly identical with those for $Fd_{9/2}$. This observation suggests that $Fd_{1/2}$ has been converted to an $Fd_{9/2}$-like state. The collapse of the magnetic hyperfine splittings at high temperature excludes Mössbauer spectroscopy as a reliable investigative tool for testing this hypothesis. However, the large change in the magnetic moment that would accompany a spin conversion from $S = {}^1/_2$ to ${}^9/_2$ turned magnetic susceptibility measurements into a decisive tool for investigating the nature of the localization-to-delocalization transition in $Fd_{1/2}$. In Figure 5A, the magnetization data collected above 80 K are displayed in a $\chi_{para}T$ plot.

For testing the spin conversion hypothesis, we have expressed $\chi_{para}$ as a weighted sum of the molar quantities (see above). A conversion of $S = {}^1/_2$ to ${}^9/_2$ would lead to an increase in $\chi$ by a factor of 33, because at high temperature $\chi_i \propto S(S+1)$. By combining this factor with the temperature-dependent molar fractions, $n_i$, listed in Table 3 ($i$ = localized or delocalized), we obtained the theoretical curve indicated by the broken line in Figure 5A. The curve lies far outside the error margins, and, therefore, the hypothesis of a spin conversion must be rejected. We conclude that the delocalized species observed at high-temperature originates from $Fd_{1/2}$ molecules which preserve their $S = {}^1/_2$ ground state.

The $\chi T$ values at high temperature are virtually temperature independent, and, within the uncertainties of our data,[35] we estimated minimum values for the energy separation between the ground and excited states: $\Delta_{3/2-1/2} > 60\ cm^{-1}$ for $Fd_{1/2}$ and $\Delta_{7/2-9/2} > 130\ cm^{-1}$ for $Fd_{9/2}$.

## Discussion

The present study has provided, for the first time, a set of hyperfine parameters for a valence-delocalized $[2Fe-2S]^+$ cluster. We have also presented evidence for a localization-to-delocalization transition for $Fd_{1/2}$ between 100 and 200 K. In the following sections we discuss briefly the hyperfine parameters for the $Fd_{9/2}$ cluster and describe a theoretical framework for understanding the nature of the transition in $Fd_{1/2}$.

**Hyperfine Parameters for $Fd_{9/2}$.** It is common practice to verify spin-coupling models by comparing the hyperfine parameters calculated for the paramagnetic sites of polynuclear clusters with the experimental values.[36,37] Thereby, the isotropic parts of the hyperfine tensors for $FeS_4$ sites in proteins and model complexes are usually adopted as the intrinsic hyperfine values for $Fe^{2+}$ and $Fe^{3+}$. The presence of clusters with different delocalization properties in our samples offers the opportunity to analyze the effect of delocalization on the hyperfine parameters of $Fd_{9/2}$ using the local site values of $Fd_{1/2}$.

For $Fd_{1/2}$, the **A**-tensors for the coupled $S = {}^1/_2$ ground state are related to the intrinsic **a**-tensors for the $Fe^{3+}$ and $Fe^{2+}$ sites by

$$\mathbf{A}_{1/2}^{3+} = ({}^7/_3)\mathbf{a}^{3+} \qquad \mathbf{A}_{1/2}^{2+} = -({}^4/_3)\mathbf{a}^{2+} \tag{2}$$

For the delocalized $Fd_{9/2}$ system, the **A**- and EFG-tensors can be written as

$$\mathbf{A_{9/2}} = \frac{1}{2}[({}^5/_9)\mathbf{a}^{3+} + ({}^4/_9)\mathbf{a}^{2+}] \tag{3}$$

$$\mathbf{V_{9/2}} = (\mathbf{V}^{3+} + \mathbf{V}^{2+})/2 \tag{4}$$

The intrinsic **a**-tensors can be transferred between eqs 2 and 3, provided the extra electron in $Fd_{9/2}$ resides in an orbital which is a linear combination of the orbitals that accommodate the electron of $Fd_{1/2}$.

The relative orientation of the principal axes of the **A**- and EFG-tensors at each site of $Fd_{1/2}$ was established by Mössbauer analysis. By contrast, the relative orientation of the tensors for the ferric and ferrous sites cannot be determined for samples

(35) The $\chi T$ values determined at 1 and 2 T do not show any temperature dependence. At 0.5 and 4 T, we found a slight temperature dependence with slopes +0.015 and −0.010 $\mu J/T^2$, respectively. These slopes were taken into account in the estimates for $\Delta_{3/2-1/2}$ and $\Delta_{7/2-9/2}$.

(36) Bominaar, E. L.; Hu, Z.; Münck, E.; Girerd, J.-J.; Borshch, S. A. *J. Am. Chem. Soc.* **1995**, *117*, 6976−6989.

(37) Papaefthymiou, V.; Girerd, J.-J.; Moura, I.; Moura, J. J. G.; Münck, E. *J. Am. Chem. Soc.* **1987**, *109*, 4703−4710.

containing randomly oriented molecules because the Zeeman term for $Fd_{1/2}$ is nearly isotropic ($g_1 = 1.88$, $g_2 = 1.92$, $g_3 = 2.01$). Assuming collinearity, there are six ways in which the Cartesian components ($x,y,z$) of the **A**- and EFG-tensors for the $Fe^{2+}$ site can be lined up with those for the $Fe^{3+}$ site in a common frame of reference. Comparison of the values for $\Delta E_Q$ and $\eta$ for $Fd_{9/2}$ calculated with eq 4 for these spatial alignments from the EFG components for the $Fd_{1/2}$ sites with the experimental values, $\Delta E_Q = +1.8$ mm/s and $\eta = 0$, provides a means to assess the relative orientations. The assignment selected in Table 2 yields $\Delta E_Q = +2.2$ mm/s and $\eta = 0.1$ for $Fd_{9/2}$, in fair agreement with the experimental values. The other possible alignments gave unsatisfactory results.

Using the assignments in Table 2, we obtain from eqs 2 and 3 for the **A**-tensor components of $Fd_{9/2}$ the values (−10.2, −10.2, −6.9) MHz, and $A^{iso}_{9/2} = (A_x + A_y + A_z)/3 = -9.1$ MHz. While the relative values of the calculated $A_{9/2}$-values follow the pattern observed experimentally, their magnitudes are about 25% smaller than the experimental ones (see Table 2). Interestingly, if we calculate $A^{iso}_{9/2}$ by using the $a^{iso}$-values of ferric (−23.4 MHz) and ferrous (−22.5 MHz) rubredoxin,[37,38] we obtain $A^{iso}_{9/2} = -11.0$ MHz, in good agreement with $A^{iso}_{9/2} = -11.6$ MHz obtained experimentally. We do not know why use of the $a$-values of $Fd_{1/2}$ yields $A_{9/2}$-values substantially lower than observed. A possible explanation for the mismatch involves the assumption that the iron sites of $Fd_{1/2}$ are more covalent than those of $Fd_{9/2}$. Alternatively, as the magnetic hyperfine tensor of the ferrous site contains a substantial orbital contribution that lowers $A^{iso}$,[39] an effective reduction of spin−orbit mixing in the delocalized $Fd_{9/2}$ system would result in a larger $a^{iso}$ contribution of the ferrous site.

The hyperfine parameters of $Fd_{1/2}$ observed for the WT protein and the C56S variant are quite unusual. Thus, for both species, the magnetic hyperfine tensor of the $Fe^{2+}$ site is nearly axial with $|A_x| \sim |A_y| > |A_z|$, in contrast to the commonly observed order $|A_z| > |A_x|, |A_y|$. Table 2 shows that the direction of the smallest **A**-tensor component coincides with that of the largest EFG-tensor component. Such a combination of EFG- and **A**-tensor components indicates a ground orbital state with an oblate ($d_{x^2-y^2}$) shape. A ligand-field analysis of these data is in progress, and we defer a discussion to a future publication. Presently, we only contrast the hyperfine parameters for plant-type ferredoxins which indicate a prolate ($d_{z^2}$) orbital ground state with our findings for the hyperfine parameters of $Fd_{1/2}$. The distinct orbital structure of the cluster in 2Fe*Cp*Fd may be one of the factors that give rise to the propensity of the mixed-valence clusters in this protein toward spin-level reordering (in $Fd_{9/2}$) and temperature-induced valence delocalization (in $Fd_{1/2}$). However, as neither of these phenomena was found to exist in the WT cluster of 2Fe*Cp*Fd, it follows that the presence of an oblate orbital state is not a sufficient condition for their existence.

**Localization-to-Delocalization Transition in $Fd_{1/2}$.** The high-temperature Mössbauer studies of samples containing a mixture of $Fd_{1/2}$ and $Fd_{9/2}$ showed that the $Fd_{1/2}$ population, or a fraction thereof, undergoes a localization-to-delocalization transition as a function of temperature, without changing the ground-state spin. Analysis of the Mössbauer spectra in the transition range (90−200 K) reveals two significant features. First, at all temperatures, the spectra consist of a superposition of three doublets, namely those for $Fe^{3+}$, $Fe^{2+}$, and $Fe^{2.5+}$ (see Figures 2 and 3, and Table 2). Significantly, the $\Delta E_Q$-values of the three doublets do not change with the temperature. Second, the intensities of the subspectra for the $Fe^{3+}$ and $Fe^{2+}$ species decrease over a broad temperature interval with concomitant increase in the intensity of the valence-averaged $Fe^{2.5+}$ subspectrum. The first feature distinguishes the localization-to-delocalization transition from frequently observed transitions which proceed by merging of the quadrupole doublets for $Fe^{2+}$ and $Fe^{3+}$ into a valence-averaged $Fe^{2.5+}$ doublet.[12,40,41] Merging (similar to exchange narrowing in NMR spectroscopy) occurs at temperatures for which the rate constant of the thermally activated ET process and, implicitly, the fluctuation rate of the electric hyperfine field are approximately equal to the nuclear precession frequencies ($\sim 10^7$ s$^{-1}$). The second feature distinguishes the delocalization phenomena in $Fd_{1/2}$ from transitions in crystalline solids, where a valence-averaged spectral component appears over a narrow temperature interval ($\Delta T = 1-2$ K).[42] The latter phenomena have been ascribed to a phase transition which originates from cooperative cluster−cluster interactions in closely packed aggregates.[42−44] For frozen protein solutions, however, the cluster−cluster separations are considerably larger, ruling out cooperative mechanisms as an explanation for our observations.

If the delocalized $Fd_{1/2}$ fraction were to be accounted for by populating delocalized excited states (with $S > {}^1/_2$), then the $S = {}^3/_2$ and $S = {}^5/_2$ levels would have to acquire a sizable population. This would lead to a considerable increase in $\chi_{para}T$ (e.g., 3.5 $\mu$J K T$^{-2}$ between 50 and 200 K for the sample of Figure 5), an increase incompatible with susceptibility data.[35]

A number of studies have identified protein dynamics as a factor relevant to long-range ET. For example, the concomitant increases in ET rate and $\langle x^2 \rangle_{Fe}$ observed above 200 K in studies of photosynthetic membranes led Chernavskii et al. to propose that segmental mobility affects ET.[45] To investigate this possibility, we have measured the temperature dependence of $\langle x^2 \rangle_{Fe}$ and observed, indeed, a sudden increase in the slope above 200 K (Figure 4), as is found in other iron proteins.[14] However, the onset of segmental motion cannot be the cause of changes in intramolecular ET rate because the transition to delocalization of $Fd_{1/2}$ starts at temperatures below 100 K and is almost complete at 200 K.

**Theoretical Model.** Essential information about the nature of the ET process can be inferred from the spectroscopic features of the localization-to-delocalization transition observed in our samples. Because the susceptibility data rule out a change in the ground-state spin of $Fd_{1/2}$, the transition is most likely due to thermal contributions to the ET process from excited states;[46] these include both vibronic and spin states. If ET for the $Fd_{1/2}$ population could be described by one (temperature-dependent) rate constant, an attendant Mössbauer spectroscopic feature of

(38) Mouesca, J.-M.; Noodleman, L.; Case, D. A.; Lamotte, B. *Inorg. Chem.* **1995**, *34*, 4347−4359.

(39) For ferrous rubredoxin, the orbital contribution to $a^{iso}$ is ca. +11 MHz.[38]

(40) Ding, X.-Q.; Bill, E.; Trautwein, A. X.; Winkler, H.; Kostikas, A.; Papaefthymiou, V.; Simopoulos, A.; Beardwood, P.; Gibson, J. F. *J. Chem. Phys.* **1993**, *99*, 6421−6428.

(41) Maeda, Y.; Tanigawa, Y.; Matsumoto, N.; Oshio, H.; Suzuki, M.; Takashima, Y. *Bull. Chem. Soc. Jpn.* **1994**, *67*, 125−130.

(42) Woehler, S. E.; Witterbort, R. J.; Oh, S. M.; Kambara, T.; Hendrickson, D. N.; Inniss, D.; Strouse, C. E. *J. Am. Chem. Soc.* **1987**, *109*, 1063−1072.

(43) Tsukerblat, B. S.; Klokishner, S. I. *Chem. Phys. Lett.* **1993**, *203*, 55−60.

(44) Linares, J.; Boukheddaden, K.; Varret, F. *Chem. Phys.* **1994**, *182*, 225−235.

(45) Chernavskii, D. S.; Frolov, E. N.; Goldanskii, V. I.; Kononenko, A. A.; Rubin, A. B. *Biophysics* **1980**, *77*, 7218−7221.

(46) Brunschwig, B. S.; Logan, J.; Newton, M. D.; Sutin, N. *J. Am. Chem. Soc.* **1980**, *102*, 5798−5809.

a localization-to-delocalization transition would be a merging of the quadrupole doublets for the $Fe^{2+}$ and $Fe^{3+}$ sites into a valence-delocalized doublet. The disparity between this prediction and our experimental findings can be resolved if we assume that $Fd_{1/2}$ represents an ensemble of molecules with a distribution in the values for the ET rate $k_{ET}$. For a quantitative analysis of our variable-temperature data, we need to specify the distribution of $k_{ET}$ at each temperature in the transition range. The temperature dependence of the rate constant can be parametrized by a small number of molecular constants.[2] These constants include $\beta$ for spin-dependent resonance interaction, $J$ for HDvV exchange, and $\chi_{reorg}$ for reorganization energy.[47]

Based on the $\langle x^2\rangle_{Fe}$ analysis, which indicates that the $Fd_{1/2}$ population in the transition range is frozen in a static distribution of conformations, it is reasonable to assume that the values of the cluster parameters are also given by temperature-independent distributions below 200 K. To evaluate the effect of dispersion in the values for $\beta$, $J$, and $\chi_{reorg}$, we have adopted an existing theoretical model for calculating tunneling rates.[2,50−52] In this model, the rate constant is the sum of Boltzmann-weighted rates (eq 5) associated with pairs of tunneling states (Figure 6A).

$$k_{ET} = \frac{2\pi^3}{h^2\omega_- Z}\sum_S\sum_\nu (\Delta E_{\nu,S})^2 (e^{-E_{\nu,S}^{+}/kT} + e^{-E_{\nu,S}^{-}/kT}) \quad (5)$$

$E_{\nu,S}^{+,-}$ is the energy of vibronic state $\nu$ in spin state $S$. For each spin state, the energy spectrum obtained using the Piepho−Krausz−Schatz (PKS) model[52] consists of pairs of levels $E_\nu^{+,-}$ (Figure 6A). The energy separation of a tunneling pair, $\Delta E_{\nu,S}$, depends on the electronic coupling parameter $\beta$, the angular frequency $\omega_-$ of a symmetry-breaking mode coupled to intramolecular ET, and the vibronic-coupling parameter $\lambda$. The latter two parameters determine the value of the reorganization parameter $\chi_{reorg} = 2\lambda^2\hbar\omega_-$. $Z$ is the partition function. Equation 5 is based on the transmission method of Weiner[50,51] and should not be confused with the method of the quantum beats, which yields much too high transfer rates when "thermal" interactions are significant.[52] Thus, the terms in eq 5 comprise the transmission coefficient $\pi^2(\Delta E_{\nu,S}/\hbar\omega_-)^2$ for a single passage of resonance $(\nu,S)$ multiplied by the number of passages per unit of time, $\omega_-/2\pi$, instead of the beat rate $\Delta E_{\nu,S}/h$.

In principle, the dynamic properties of a mixed-valence system observed in a Mössbauer experiment depend on four time scales, i.e., those for transitions between localized states with different spin or vibronic quantum numbers ($\tau_{loc}$), transitions between the magnetic sublevels of a spin multiplet ($\tau_{para}$), intervalence transitions in which the extra electron moves between the metal sites ($\tau_{ET}$), and the precession times ($\tau_{Mö}$) of the Mössbauer nucleus, which depend on the hyperfine interactions at the $Fe^{2+}$ and $Fe^{3+}$ sites. At temperatures in the transition range, the magnetic hyperfine interactions are collapsed, $\tau_{para} < \tau_{Mö}$. Hence, $\tau_{para}$ can be ignored in our considerations. However, $\Delta E_Q$ and $\delta$, as electrostatic parameters, are not affected by paramagnetic relaxation but depend on the relative magnitude of $\tau_{ET}$ and $\tau_{Mö}$. The transmission method is based on the assumption that the lifetime of a localized state is short compared to the time for electron transfer, $\tau_{loc} \ll \tau_{ET}$.[50] Concomitantly, by adopting a thermally averaged rate constant (eq 5), we have implicitly assumed that the lifetimes of states

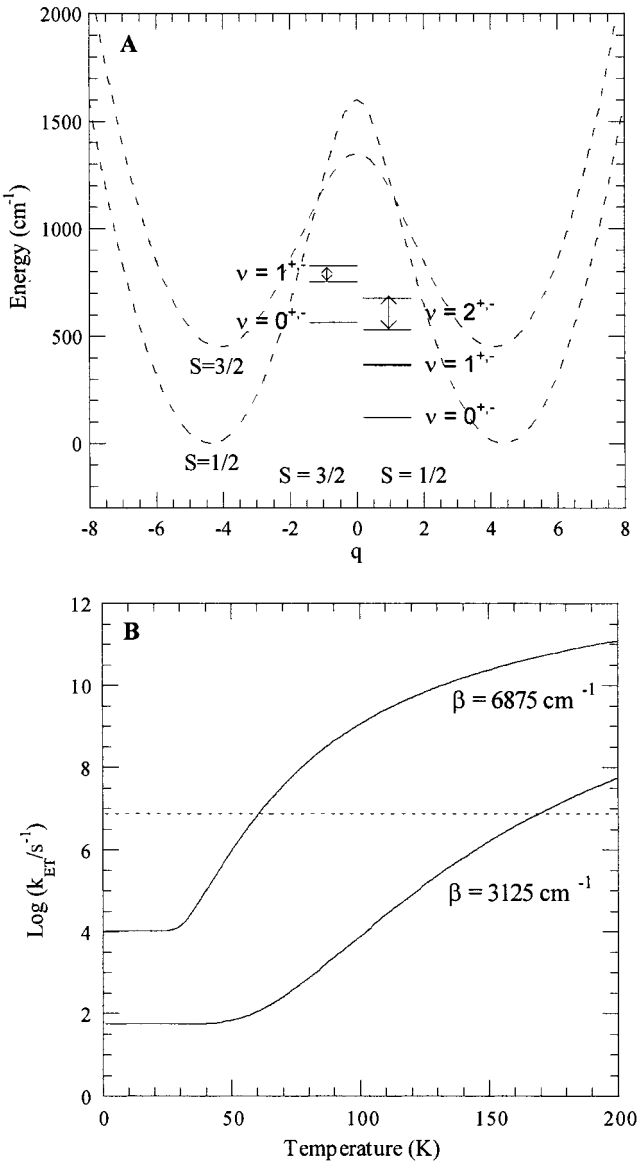


**Figure 6.** (A) The middle part of the plot represents energies of the first vibronic levels of the $S = {}^1/_2$ and ${}^3/_2$ states calculated using the PKS model for a multispin system with spin-dependent resonance parameter $\beta_S = \beta(S + {}^1/_2)/5$ and, in the presence of HDvV exchange, $-2J\mathbf{S}_1\cdot\mathbf{S}_2$. Parameters used: $\lambda = 4$, $\hbar\omega_- = 300$ cm$^{-1}$, $\beta = 5000$ cm$^{-1}$, $J = -250$ cm$^{-1}$. The energy differences between pairs of vibronic levels were multiplied by $10^4$ for the $S = {}^1/_2$ state and by $10^3$ for the $S = {}^3/_2$ state. The double-well potentials (hashed lines) were calculated in semiclassical approximation using the same parameters. (B) Temperature dependence of the ET rate calculated using eq 5, for $J = -290$ cm$^{-1}$, $\hbar\omega_- = 300$ cm$^{-1}$, $\chi_{reorg} = 9600$ cm$^{-1}$, and $\beta = 3175$ or 6875 cm$^{-1}$. The hashed line approximately represents the $^{57}$Fe nuclear precession rate.

(47) Hendrickson and collaborators[12] have proposed that the quenching of electron tunneling observed in a number of molecular mixed-valence crystals is due to the mismatch of the vibronic levels at the inequivalent metal sites of a dimer. However, in the framework of a multiphonon theory for ET in proteins,[48] such a mismatch is of little consequence if the system is effectively coupled to a bath of low-frequency modes. Vibrational spectra of proteins differ significantly from those for solids; while proteins have a high spectral density at the low end of the frequency scale,[49] the phonon density in solids goes to zero as a quadratic function of the frequency. For this reason, we have adopted the view, albeit tentatively, that the distribution in ET rate does not originate from a distribution in the site differentiation energy.

(48) Ulstrup, J.; Jortner, J. *J. Chem. Phys.* **1975**, *63*, 4358−4368.
(49) Basu, G.; Kitao, A.; Go, N. *J. Phys. Chem. B* **1998**, *102*, 2076−2084.
(50) Weiner, J. H. *J. Chem. Phys.* **1978**, *69*, 4743−4749.
(51) Weiner, J. H. *J. Chem. Phys.* **1978**, *68*, 2492−2506.
(52) Wong, K. Y.; Schatz, P. N. *Prog. Inorg. Chem.* **1981**, *28*, 369−449.

involved in the ET process are short on the Mössbauer time scale, i.e., $\tau_{loc} \ll \tau_{Mö}$.

The latter two assumptions about $\tau_{loc}$ are certainly fulfilled for the vibronic states ($\tau_{vib} \approx 10^{-10}-10^{-12}$ s). The spin states are longer lived than the vibronic states but probably not to the extent as to invalidate our approach. The latter view is supported by the fast paramagnetic relaxation observed in the transition region, especially if we assume that the relaxational processes are of the indirect (e.g., Orbach) type. We note that each spin state with a long lifetime compared to $\tau_{Mö}$ would contribute a spectrum with delocalization characteristics depending on the magnitude of the rate constant for that particular state, $k_{ET}(S)$. However, in our experiments, long-lived excited spin states can only account for a minor fraction of the net Mössbauer absorption in $Fd_{1/2}$ because the thermal population of states with $S > {}^1/_2$ was found to be negligibly small.

For short lifetimes such as those encountered here, the rates for the ground and excited states can be combined into a single rate constant (as expressed in eq 5), which can be compared with the relevant nuclear precession frequencies to decide whether a molecule is delocalized or not (i.e., localization for $\tau_{ET} < \tau_{Mö}$ and delocalization for $\tau_{ET} > \tau_{Mö}$). It is important to note that contributions to $k_{ET}$ from short-lived excited spin states which have high electron-transfer rates can have an appreciable effect on the Mössbauer spectra, despite the smallness of their Boltzmann factors. Thus, even minutely occupied excited spin states can cause spectroscopic valence delocalization, provided there is a sufficiently fast relaxational communication between the states.

Figure 6A depicts the energies of the first few vibronic levels of the $S = {}^1/_2$ and ${}^3/_2$ states calculated using the PKS model with spin-dependent resonance parameter $\beta_S = \beta(S + {}^1/_2)/5$ in the presence of HDvV exchange, $-2J\mathbf{S}_1\cdot\mathbf{S}_2$. Also shown are the semiclassical double-well potentials which indicate that $Fd_{1/2}$ is class II according to Robin and Day classification in its lower spin states (class III, the strong resonance case, corresponds to a single well). The figure shows that the energy splitting of low-lying pairs of tunneling states is small and increases with the vibrational and spin quantum numbers. The considerably greater efficiency of ET via states with $S > {}^1/_2$ determines a steep increase of the ET rate with temperature (see Figure 6B).

Molecules with different values for the cluster parameters have $k_{ET}$ vs $T$ curves that cross the critical nuclear precession frequencies at different temperatures. This dispersion of the transition temperatures is illustrated in Figure 6B for two different values of the resonance interaction parameter $\beta$. Because at any temperature in the transition range there are molecules with rates well above and below $\tau_{Mö}$, the Mössbauer spectra appear as a superposition of localized and delocalized spectral components. For an ensemble of molecules with a wide distribution of ET rates, only a minority fraction of clusters has ET rates in the frequency domain corresponding to intermediate relaxation. For this reason, a meaningful analysis of the high-temperature spectra does not necessarily require elaborate simulations of intermediate relaxation behavior. Moreover, apart from accounting for line shape effects associated with ET, a relaxation analysis has to include residual paramagnetic relaxation in order to be complete. This would introduce inevitably the concern of overparametrization. Figure 7 shows the calculated temperature dependence of the molecular fraction delocalized on the Mössbauer time scale for the sample of Figures 1 and 2. This curve was obtained by using eq 5 and assuming an equiprobable distribution in the $\beta$-values between 3125 and 6875 cm$^{-1}$ and zero elsewhere, while keeping the other parameters fixed at a given value ($J = -290$ cm$^{-1}$, $\chi_{reorg} = 9600$ cm$^{-1}$, $\hbar\omega_- = 300$ cm$^{-1}$). The width of the temperature interval over which the transition occurs and the type of temperature dependence are determined by the shape of the $\beta$-distribution. In the same vein, distributions in $\chi_{reorg}$ and $J$ can also be used for simulating our experimental data.[53]

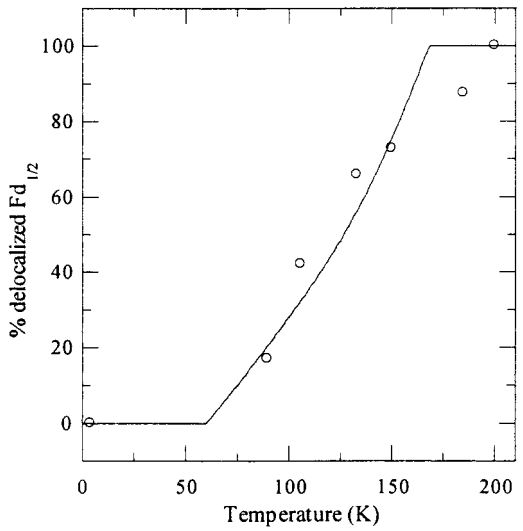


**Figure 7.** Experimental and calculated temperature dependence of the fraction of delocalized $Fd_{1/2}$ (42% of the clusters in the sample at 200 K). These experimental data (○) were normalized to 100% delocalized $Fd_{1/2}$ at 200 K. The calculated temperature dependence of the fraction of delocalized $Fd_{1/2}$ clusters was obtained using the theoretical model described in the text and assuming a constant probability $\beta$-distribution between $\beta = 3175$ and 6875 cm$^{-1}$. Other parameters: $J = -290$ cm$^{-1}$, $\hbar\omega_- = 300$ cm$^{-1}$, $\chi_{reorg} = 9600$ cm$^{-1}$.

The dispersions in the cluster parameters required for explaining the Mössbauer features of the localization-to-delocalization transition are rather large when compared with the spread in the exchange-coupling constants for synthetic [2Fe−2S]$^{2+}$ clusters.[54,55] In contrast to the exchange-coupling constants for the diferric clusters, the $J$-values reported for protein-bound [2Fe−2S]$^{+}$ clusters show much greater variation.[56] In addition, the existence of the $Fd_{1/2}$ and $Fd_{9/2}$ species demonstrates that [2Fe−2S]$^{+}$ clusters can sustain a complete reordering of the spin levels, supporting the notion that cluster−protein interactions can have a considerable impact on the exchange parameters.

The proposal that distributions of protein conformation determine variations in the electronic structure of the mixed-valence clusters probed in the high-temperature Mössbauer studies is also supported by the finding that $Fd_{1/2}$ clusters in the lyophilized sample do not exhibit a localization-to-delocalization transition.

## Conclusions

The studies described here reveal novel properties of the [2Fe−2S]$^{+}$ clusters in the C56S variant 2Fe*Cp*Fd. Hyperfine

(53) Constant distributions in $\chi_{reorg}$ between 7150 and 11 350 cm$^{-1}$ (for $J = -255$ cm$^{-1}$, $\beta = 5000$ cm$^{-1}$, and $\hbar\omega_- = 300$ cm$^{-1}$) or in $J$ −100 and −400 cm$^{-1}$ (for $\beta = 5000$ cm$^{-1}$, $\chi_{reorg} = 9600$ cm$^{-1}$, and $\hbar\omega_- = 300$ cm$^{-1}$) can also describe the data. The quality of the latter simulation is lower than that of the simulations obtained for distributions in $\beta$ and $\chi_{reorg}$, most likely because changes in $J$ affect only the relative contributions of different tunneling levels to $k_{ET}$ and not the values of the individual $k_{ET}(S)$.

(54) Gillum, W. O.; Frankel, R. B.; Foner, S.; Holm, R. H. *Inorg. Chem.* **1976**, *15*, 1095−1100.

(55) Wong, G. B.; Bobrik, M. A.; Holm, R. H. *Inorg. Chem.* **1978**, *17*, 578−584.

(56) Lloyd, S. G.; Franco, R.; Moura, J. J. G.; Moura, I.; Ferreira, G. C.; Huynh, B. H. *J. Am. Chem. Soc.* **1996**, *118*, 9892−9900.

parameters of these clusters point to a ground orbital state different from that for $[2Fe-2S]^{+}$ clusters in plant-type ferredoxins. The clusters in our samples show the first localization-to-delocalization transition ever observed for a biological cluster. During the transition, there is coexistence of localized and delocalized species which we tentatively ascribe to the influence of heterogeneous protein environments on the cluster. The sensitivity of the rate for intracluster ET to the protein environment reinforces the notion that proteins can tune the biological function of clusters[7] and suggests the possibility of using Fe−S clusters as sensors for the conformation of the coordinating protein.

**Acknowledgment.** This research was supported by National Science Foundation Grant MCB-9406224 to E.M.

JA983980K